JACS
JOURNAL OF THE AMERICAN CHEMICAL SOCIETY

pubs.acs.org/JACS

Communication

Short-Wave Infrared Upconverting Nanoparticles

Xiao Qi, Changhwan Lee, Benedikt Ursprung, Artiom Skripka, P. James Schuck,* Emory M. Chan,* and Bruce E. Cohen*

Cite This: *J. Am. Chem. Soc.* 2024, 146, 29292−29296

Read Online

ACCESS | Metrics & More | Article Recommendations | Supporting Information

ABSTRACT: Optical technologies enable real-time, noninvasive analysis of complex systems but are limited to discrete regions of the optical spectrum. While wavelengths in the short-wave infrared (SWIR) window (typically, 1700−3000 nm) should enable deep subsurface penetration and reduced photodamage, there are few luminescent probes that can be excited in this region. Here, we report the discovery of lanthanide-based upconverting nanoparticles (UCNPs) that efficiently convert 1740 or 1950 nm excitation to wavelengths compatible with conventional silicon detectors. Screening of Ln^{3+} ion combinations by differential rate equation modeling identifies Ho^{3+}/Tm^{3+} or Tm^{3+} dopants with strong visible or NIR-I emission following SWIR excitation. Experimental upconverted photoluminescence excitation (U-PLE) spectra find that 10% Tm^{3+}-doped $NaYF_4$ core/shell UCNPs have the strongest 800 nm emission from SWIR wavelengths, while UCNPs with an added 2% or 10% Ho^{3+} show the strongest red emission when excited at 1740 or 1950 nm. Mechanistic modeling shows that addition of a low percentage of Ho^{3+} to Tm^{3+}-doped UCNPs shifts their emission from 800 to 652 nm by acting as a hub of efficient SWIR energy acceptance and redistribution up to visible emission manifolds. Parallel experimental and computational analysis shows rate equation models are able to predict compositions for specific wavelengths of both excitation and emission. These SWIR-responsive probes open a new IR bioimaging window, and are responsive at wavelengths important for vision technologies.

For a century after the synthesis of the first fluorescent molecules,[1] luminescent probes were developed largely to emit at visible or ultraviolet wavelengths, enabling easy detection by eye and early detectors. The realization that longer wavelengths hold major advantages in imaging and optical technologies has sparked interest in probes in the near-infrared (NIR, 700−1700 nm) and short-wave infrared (SWIR, 1700−3000 nm), although there is wide variation in defining these ranges.[2−6] In biological imaging, NIR wavelengths have been shown to be less phototoxic, scatter less in tissue, and do not generate significant autofluorescence (Figure 1a).[2,7−9] For solar and passive night vision technologies, more efficient NIR-II and SWIR probes could enable the harvesting of sunlight and nighttime atmospheric luminescence (*i.e.*, nightglow) at wavelengths that have been untapped for use in optical technologies (Figure 1b).[10]

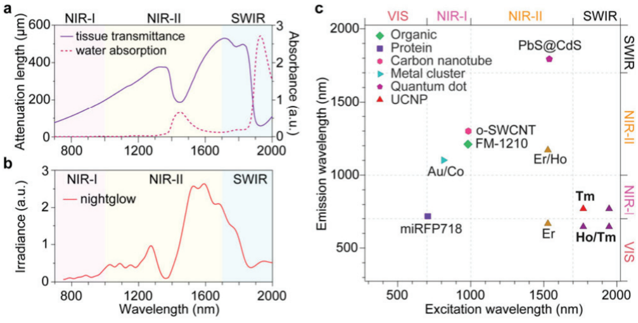

Figure 1. Applications and probes in the SWIR. (a) Calculated attenuation length of brain tissue[4] and water absorption[14] in the NIR and SWIR. (b) Calculated nightglow irradiance spectrum using the Cerro Paranal sky model.[10] (c) Peak excitation and emission wavelengths of long-wavelength organic,[11] fluorescent protein,[5] carbon nanotube,[26] metal cluster,[13] quantum dot,[4] and UCNP[27,28] probes. Tm^{3+} and Ho^{3+}/Tm^{3+} UCNPs were obtained from this work.

While there has been good progress in NIR-II (1000−1700 nm) probes with organics[3,11] and nanomaterials,[4,12,13] excitation beyond 1700 nm remains largely unexplored (Figure 1c). This derives from innate limitations in the photophysics and stability of many of these probes at long wavelengths,[14] as well as the lack of commercial imaging systems for wavelengths beyond 1700 nm.[15,16] Probes that can be excited at SWIR wavelengths and emit at wavelengths compatible with conventional silicon detectors would be ideal for harnessing the SWIR spectrum and enable integration into existing optical systems.

Upconverting nanoparticles (UCNPs) are lanthanide-based phosphors that combine the energies of multiple long-wavelength photons to emit at shorter wavelengths, commonly with 980 or 800 nm excitation, and emission in the visible or NIR-I. UCNPs do not measurably blink or photobleach, and Ln^{3+}-based upconversion can be up to a billion-fold more efficient than the best 2-photon fluorophores.[7,17−19] Here, we extend UCNP upconversion to excitation wavelengths >1700 nm, showing that Tm^{3+} and Ho^{3+}/Tm^{3+} compositions can be

Received: August 14, 2024
Revised: October 14, 2024
Accepted: October 17, 2024
Published: October 21, 2024

ACS Publications

https://doi.org/10.1021/jacs.4c11181

excited in the SWIR to emit in NIR-I and visible regions. Aided by development of methods for calculating and measuring upconverted photoluminescence excitation (U-PLE) spectra, we find that Tm^{3+}-doped UCNPs allow for efficient 800 nm emission with 1740 nm excitation, while addition of low concentrations of Ho^{3+} promotes 652 nm emission with either 1740 or 1950 nm excitation. These methods for U-PLE engineering and the resultant SWIR-responsive probes open a new IR bioimaging window and are responsive at important spectral regions for night vision technologies.

To find Ln^{3+} combinations able to upconvert SWIR excitation, we developed a high-throughput method to calculate thousands of U-PLE and emission spectra for UCNPs doped with any combination of Ln^{3+} ions (Figure 2), using differential rate equation (DRE) models of Ln^{3+} photophysics[20−22] that have successfully predicted UCNP excitation and emission profiles (see Methods for modeling details).[23−25] U-PLE spectra were extracted from 2D spectral maps (Figure S1) generated by calculating the emission spectra for each excitation wavelength in a specified range. We first calculated the U-PLE spectra for 129 combinations of 1 to 3 Ln^{3+} ions (1 mol % each), and screened for SWIR excitation peaks that give rise to emission at visible or NIR-I wavelengths (Figures 2a and S2).

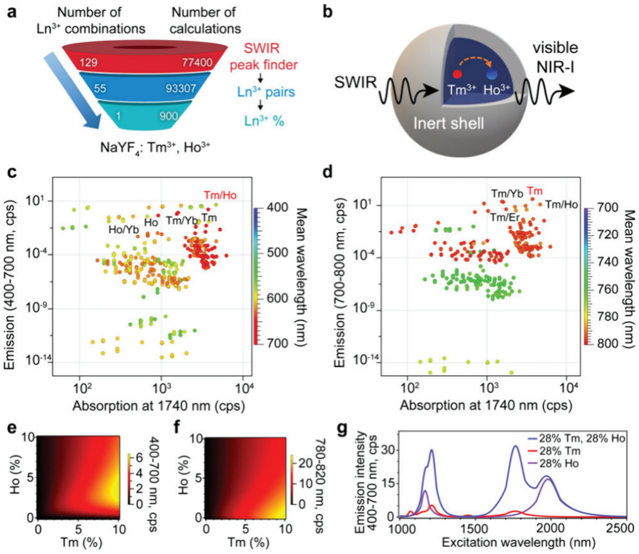

Figure 2. Computational screening of Ln^{3+} combinations for SWIR upconversion. (a) Sequential Ln^{3+} selection scheme. (b) Upconversion in Ho^{3+}/Tm^{3+} core/shell UCNPs. (c,d) DRE modeling[23−25] of 385 combinations (total Ln^{3+} concentration = 20%) for visible or NIR-I emission. (e,f) Heat maps of integrated visible or NIR-I emission for Ho^{3+}/Tm^{3+} UCNPs, excited at 1740 nm. (g) Calculated U-PLE spectra for Ho^{3+}/Tm^{3+} UCNPs. Excitation intensities were set to 100 kW/cm^2.

We then performed a secondary screen of the 55 brightest Ln^{3+} combinations in which we varied doping levels (Table S4) and screened for upconversion from U-PLE peaks. Ho^{3+}/Tm^{3+} and Tm^{3+} emerge as the brightest compositions for visible and NIR-I emission when excited at 1740 and 1950 nm (Figures 2b and S3).

To optimize emission at these excitation wavelengths, we calculated the emission spectra for 385 combinations of 1−4 dopants (Figure 2c,d). Under 1740 nm excitation, the brightest composition, 10% Tm^{3+} and 10% Ho^{3+}, shows enhanced visible emission compared with either dopant alone. For the NIR-I emission, 20% Tm^{3+} shows the strongest 800 nm emission and is quenched by codopants. Screening of both Tm^{3+} and Ho^{3+} finds that low Ho^{3+} levels mediate visible emission but this diminishes above ∼5% (Figure 2e,f). Calculated U-PLE spectra show broad excitation peaks at 1210, 1740, and 1950 nm, with large enhancements compared to those of singly doped UCNPs (Figure 2g), suggesting specific Tm^{3+}−Ho^{3+} interactions may amplify their response to SWIR wavelengths.

To test these DRE calculations experimentally, we synthesized 20 nm β-phase $NaYF_4$ UCNPs doped with either Tm^{3+} or Ho^{3+}/Tm^{3+}, and overcoated them with inert 5 nm $NaYF_4$ shells.[7,23] Structural characterization by high-angle annular dark-field scanning transmission electron microscopy (HAADF-STEM, Figures 3a,b and S4), energy dispersive spectrometry (EDS, Figure S5), and powder X-ray diffraction (XRD, Figure S6) show monodisperse β-phase core/shell heterostructures. To characterize their NIR-II/SWIR sensitivity, we developed an experimental technique to acquire U-PLE spectra from 1000−1600 nm and 1700−2050 nm by scanning a tunable femtosecond-pulsed optical parametric oscillator (OPO) laser and acquiring emission spectra from 430 to 950 nm (Scheme S1).

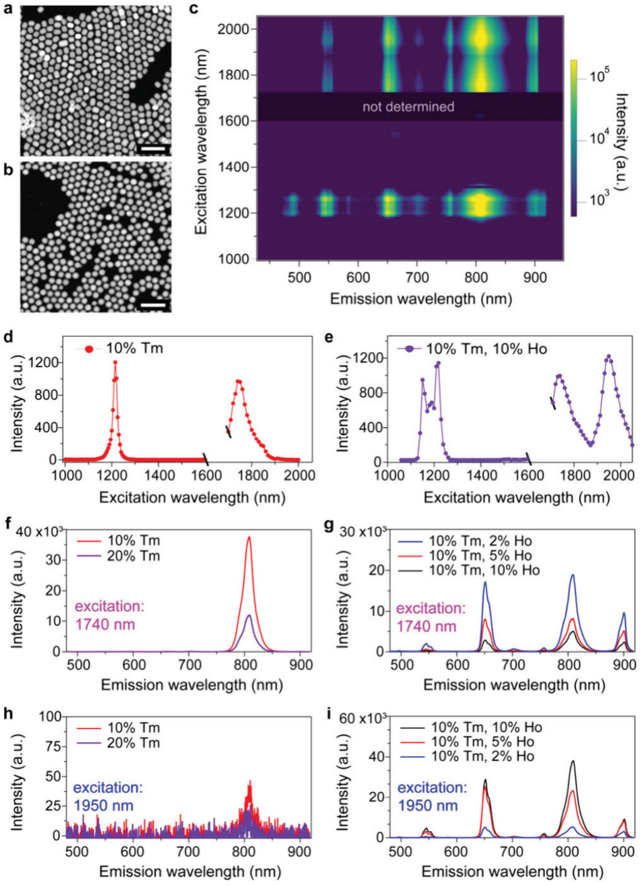

Figure 3. Experimental characterization of SWIR UCNPs. HAADF-STEM images of (a) 10% Tm^{3+} and (b) Ho^{3+}/Tm^{3+} core/shell $NaYF_4$: UCNPs. Scale bars are 100 nm. (c) 2D excitation−emission spectral map of 10% Tm^{3+}, 10% Ho^{3+} UCNPs. (d,e) U-PLE spectra of Tm^{3+} UCNP (780−820 nm emission) and Ho^{3+}/Tm^{3+} UCNP (630−670 nm emission) films. Excitation intensities are 10 kW/cm^2. Emission spectra of 1 μM dispersions in hexane of (f) Tm^{3+} and (g) Ho^{3+}/Tm^{3+} UCNPs with 1740 nm, or (h,i) 1950 nm excitation (90 kW/cm^2 for (f)−(i)).

Excitation−emission maps constructed from these data sets (Figures 3c and S1) were used for simultaneous exploration of both U-PLE and emission peaks. For 10% Tm^{3+} UCNPs, U-PLE peaks corresponding to ground state absorption (GSA: 1210 nm, 1740 nm) are apparent for 800 nm emission (Figure 3d). While Tm^{3+}-doped UCNPs that show avalanching behavior[24,29] exhibit strong excited state absorption (ESA), these peaks (1064 nm, 1450 nm) are missing here, consistent with modeling (Figures 2g and S1) that experimental power densities fall below avalanching thresholds. For Ho^{3+}/Tm^{3+} UCNPs, significant GSA peaks are observed at 1170, 1210, 1740, and 1950 nm (Figure 3e), consistent with simulated results (Figures 2g and S7), although relative U-PLE intensities vary and experimental peak features are sharper.

Tuning these compositions to optimize SWIR upconversion, we find that increasing Tm^{3+} levels beyond 10% quenches emission, and only NIR-I emission from 1740 nm excitation is observed (Figure 3f,h), whereas both visible and NIR-I emissions are elicited from Ho^{3+}/Tm^{3+} (Figure 3g). UCNPs with 10% Tm^{3+} and 2% Ho^{3+} are brightest at both red and NIR-I wavelengths, in agreement with the simulation results (Figure 2e,f and Table S5). Ho^{3+} is needed for 1950 nm upconversion to red and NIR-I emission, with 10% Tm^{3+}/10% Ho^{3+} showing the brightest emission in both ranges (Figure 3i). When excited at 1740 nm, Ho^{3+}/Tm^{3+} codoped UCNPs reveal power-dependent slope factors (n) between 2.4 and 3.1, while 1950 nm excitation shows lower n values between 2.0 and 2.6 (Figure S8).

To quantify the brightness of these UCNPs, we synthesized core−shell UCNPs doped with 10% Er^{3+}, a composition known for efficient 1550 nm-to-visible upconversion,[30] and used this to benchmark the brightness of Tm^{3+} and Ho^{3+}/Tm^{3+} SWIR upconversion (Table S5). Emission measurements of equimolar dispersions under identical conditions show a similar Er^{3+} 1550 nm-to-visible intensity to Tm^{3+} 1740 nm-to-NIR-I emission and ∼4-fold higher Er^{3+} 1550 nm-to-visible emission intensity compared to Ho^{3+}/Tm^{3+} 1740 nm-to-visible emission. Under 1950 nm excitation, the combined visible and NIR-I emission of 10% Tm^{3+}/10% Ho^{3+} UCNPs exceeds that of 10% Er^{3+} UCNPs under 1550 nm excitation (Table S5).

To better understand the mechanisms of SWIR upconversion, we carried out DRE analysis to determine the main energy transfer (ET) pathways in these UCNPs (Figures 4, S9−S10 and Tables S7−S8). Under 1740 nm excitation, the Tm^{3+}:$^3F_4$ manifold is predominantly populated via resonant GSA (Figure 4a), which drives SWIR → NIR-I upconversion by serving as a donor for the dominant energy transfer upconversion (ETU, steps 1−2) pathway that populates the 800 nm-emitting $^3H_4$ level. Addition of Ho^{3+} introduces ET pathways that enhance visible emission (Figure 4b), including from Tm^{3+}:$^3F_4$ to Ho^{3+}:$^5I_7$, which then drives ETU that progressively excites Ho^{3+} and Tm^{3+} up to visible or NIR-I emitting states. When excited at 1950 nm, Ho^{3+} acts as the primary sensitizer, as Ho^{3+}:$^5I_7$ is directly populated by GSA (Figure S11), and this allows ET to Tm^{3+}:$^3H_4$ for NIR-I emission.

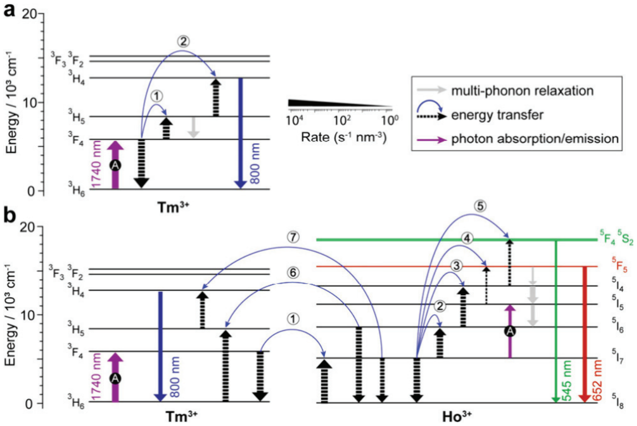

Figure 4. Mechanisms of SWIR upconversion. Key pathways of (a) 10% Tm^{3+} and (b) Ho^{3+}/Tm^{3+} UCNPs. Processes are simplified for clarity; more complete mechanisms are listed in Figures S9 and S11.

For many applications, SWIR excitation wavelengths would have clear advantages over the NIR and visible wavelengths, including lower phototoxicity, greater subsurface penetration, and alignment with ambient radiation sources. The penetration depth through tissue at 1740 nm is almost 5-fold deeper than at 800 nm (Figure 1a), a wavelength commonly used for deep-tissue imaging. The 1740 nm excitation wavelength may be most useful for imaging and optical technologies where water is present, as 1950 nm coincides with a water absorbance peak, whereas 1740 nm lies between water peaks.[14]

Organic fluorophores with NIR-II excitation have shown impressive ability to be imaged with high contrast at video rates deep in live animals, even with relatively modest quantum yields.[3,31,32] Nanostructures with NIR-II excitation, including carbon nanotubes[12,26] and semiconductor QDs,[4] have also found use for deep-tissue imaging experiments. Despite these advances in probe chemistry, the major roadblock has been detector sensitivity and noise,[16] and there are few practical options for Stokes-shifted emission above 1700 nm.[33]

Previous work has shown 1550 nm excitation of Er^{3+}-based UCNPs[27,28] and 1450 nm for Tm^{3+}-based avalanching nanoparticles,[24] but apparently not from longer excitation wavelengths. To address this, we have developed computational and experimental methods for unbiased screening of SWIR upconversion. A DRE screen involving over 200,000 calculations identifies Tm^{3+} and Ho^{3+}/Tm^{3+} as prime candidates, and emission measurement from these UCNPs with 1740 or 1950 nm excitation are comparable to Er^{3+}-based UCNP emission excited with 1550 nm (Table S5), suggesting pathways around the quenching processes often encountered in codoped UCNP systems.[34−36] This obviates the need to isolate dopants within multishell heterostructures,[29] which necessarily increase synthetic complexity and probe size.

A quantitative comparison between calculated and measured emissions shows that DRE models are adept at predicting Ln^{3+} combinations and approximate doping percentages. Model predictions of peak ratios and power dependence may be improved by incorporating experimental absorption lineshapes[20−22] and nonidealized dopant distributions and nanocrystal structures.[37,38]

In energy transfer upconversion, n is primarily a function of the ETU and decay rates from intermediate levels[39−41] and represents the number of photons in an upconversion process only when decay is much faster than ETU (*e.g.*, below saturating powers). Modeling of SWIR UCNPs shows comparable ETU and decay rates from the Ho^{3+}:$^5I_7$ level (Tables S6−S8), making n values lower than might be expected for such a large energy difference, but consistent with power-dependent measurements (Figure S8). In comparisons of UCNP excitation, continuous wave lasers have shown brightness several orders of magnitude higher compared to pulsed systems[42] like the 80 MHz OPO laser used here, suggesting room for improved SWIR UCNP brightness. These initial SWIR compositions begin the process of developing imaging,[7,19] sensing,[43] and optical memory[44] systems that operate far beyond current wavelengths.

■ ASSOCIATED CONTENT

Supporting Information

The Supporting Information is available free of charge at https://pubs.acs.org/doi/10.1021/jacs.4c11181.

Experimental and computational methods, a microscope scheme, simulated and experimental spectral data, nanoparticle structural characterization, and additional mechanistic data (PDF)

Machine-readable simulation data, including nanoparticle compositions and spectral outcomes (TXT)

■ AUTHOR INFORMATION

Corresponding Authors

P. James Schuck − *Department of Mechanical Engineering, Columbia University, New York, New York 10027, United States;* orcid.org/0000-0001-9244-2671; Email: p.j.schuck@columbia.edu

Emory M. Chan − *The Molecular Foundry, Lawrence Berkeley National Laboratory, Berkeley, California 94720, United States;* orcid.org/0000-0002-5655-0146; Email: emchan@lbl.gov

Bruce E. Cohen − *The Molecular Foundry, Lawrence Berkeley National Laboratory, Berkeley, California 94720, United States; Division of Molecular Biophysics & Integrated Bioimaging, Lawrence Berkeley National Laboratory, Berkeley, California 94720, United States;* orcid.org/0000-0003-3655-3638; Email: becohen@lbl.gov

Authors

Xiao Qi − *The Molecular Foundry, Lawrence Berkeley National Laboratory, Berkeley, California 94720, United States;* orcid.org/0000-0003-4884-6454

Changhwan Lee − *Department of Mechanical Engineering, Columbia University, New York, New York 10027, United States;* Present Address: Department of Materials Science and Engineering, Korea Advanced Institute of Science and Technology, Daejeon, 34141, Republic of Korea

Benedikt Ursprung − *Department of Mechanical Engineering, Columbia University, New York, New York 10027, United States*

Artiom Skripka − *The Molecular Foundry, Lawrence Berkeley National Laboratory, Berkeley, California 94720, United States;* orcid.org/0000-0003-4060-4290

Complete contact information is available at: https://pubs.acs.org/10.1021/jacs.4c11181

Funding

U.S. Department of Defense − DARPA U.S. Department of Energy − Basic Energy Sciences U.S. National Science Foundation

Notes

The authors declare no competing financial interest.

■ ACKNOWLEDGMENTS

We are grateful to Ken Crozier and Dragomir Neshev for useful discussions. This work was supported by the Defense Advanced Research Projects Agency (DARPA) EnVision program under Contracts No. HR001111365551 (E.M.C. and B.E.C.) and HR00112220006 (P.J.S.). Work at the Molecular Foundry was supported by the Director, Office of Science, Office of Basic Energy Sciences (BES), Division of Materials Sciences and Engineering, of the U.S. Department of Energy (DOE) under Contract No. DE-AC02-05CH11231. X.Q., A.S. and E.M.C. acknowledge support from the DOE/BES under the same contract through the Chemical Sciences, Geosciences, and Biosciences Division, Separations Program. P.J.S. acknowledges support from the U.S. National Science Foundation, Grant CHE-2203510.

■ REFERENCES

(1) Baeyer, A. Ueber Eine Neue Klasse von Farbstoffen. *Ber. Dtsch. Chem. Ges.* **1871**, *4* (2), 555−558.

(2) Golovynskyi, S.; Golovynska, I.; Stepanova, L. I.; Datsenko, O. I.; Liu, L.; Qu, J.; Ohulchanskyy, T. Y. Optical Windows for Head Tissues in Near-Infrared and Short-Wave Infrared Regions: Approaching Transcranial Light Applications. *J. Biophotonics* **2018**, *11* (12), No. e201800141.

(3) Cosco, E. D.; Spearman, A. L.; Ramakrishnan, S.; Lingg, J. G. P.; Saccomano, M.; Pengshung, M.; Arús, B. A.; Wong, K. C. Y.; Glasl, S.; Ntziachristos, V.; Warmer, M.; McLaughlin, R. R.; Bruns, O. T.; Sletten, E. M. Shortwave Infrared Polymethine Fluorophores Matched to Excitation Lasers Enable Non-Invasive, Multicolour in Vivo Imaging in Real Time. *Nat. Chem.* **2020**, *12* (12), 1123−1130.

(4) Wang, F.; Ren, F.; Ma, Z.; Qu, L.; Gourgues, R.; Xu, C.; Baghdasaryan, A.; Li, J.; Zadeh, I. E.; Los, J. W. N.; Fognini, A.; Qin-Dregely, J.; Dai, H. In Vivo Non-Invasive Confocal Fluorescence Imaging beyond 1,700 nm Using Superconducting Nanowire Single-Photon Detectors. *Nat. Nanotechnol.* **2022**, *17* (6), 653−660.

(5) Oliinyk, O. S.; Ma, C.; Pletnev, S.; Baloban, M.; Taboada, C.; Sheng, H.; Yao, J.; Verkhusha, V. V. Deep-Tissue SWIR Imaging Using Rationally Designed Small Red-Shifted Near-Infrared Fluorescent Protein. *Nat. Methods* **2023**, *20* (1), 70−74.

(6) Lei, Z.; Zhang, F. Molecular Engineering of NIR-II Fluorophores for Improved Biomedical Detection. *Angew. Chem., Int. Ed. Engl.* **2021**, *60* (30), 16294−16308.

(7) Tian, B.; Fernandez-Bravo, A.; Najafiaghdam, H.; Torquato, N. A.; Altoe, M. V. P.; Teitelboim, A.; Tajon, C. A.; Tian, Y.; Borys, N. J.; Barnard, E. S.; Anwar, M.; Chan, E. M.; Schuck, P. J.; Cohen, B. E. Low Irradiance Multiphoton Imaging with Alloyed Lanthanide Nanocrystals. *Nat. Commun.* **2018**, *9* (1), 3082.

(8) Wang, F.; Zhong, Y.; Bruns, O.; Liang, Y.; Dai, H. In Vivo NIR-II Fluorescence Imaging for Biology and Medicine. *Nat. Photonics* **2024**, *18* (6), 535−547.

(9) Horton, N. G.; Wang, K.; Kobat, D.; Clark, C. G.; Wise, F. W.; Schaffer, C. B.; Xu, C. In Vivo Three-Photon Microscopy of Subcortical Structures within an Intact Mouse Brain. *Nat. Photonics* **2013**, *7* (3), 205−209.

(10) Noll, S.; Kausch, W.; Barden, M.; Jones, A. M.; Szyszka, C.; Kimeswenger, S.; Vinther, J. An Atmospheric Radiation Model for Cerro Paranal - I. The Optical Spectral Range. *Astron. Astrophys. Suppl. Ser.* **2012**, *543*, A92.

(11) Fang, Y.; Shang, J.; Liu, D.; Shi, W.; Li, X.; Ma, H. Design, Synthesis, and Application of a Small Molecular NIR-II Fluorophore with Maximal Emission beyond 1200 nm. *J. Am. Chem. Soc.* **2020**, *142* (36), 15271−15275.

(12) Welsher, K.; Liu, Z.; Sherlock, S. P.; Robinson, J. T.; Chen, Z.; Daranciang, D.; Dai, H. A Route to Brightly Fluorescent Carbon Nanotubes for Near-Infrared Imaging in Mice. *Nat. Nanotechnol.* **2009**, *4* (11), 773−780.

(13) Marbella, L. E.; Andolina, C. M.; Smith, A. M.; Hartmann, M. J.; Dewar, A. C.; Johnston, K. A.; Daly, O. H.; Millstone, J. E. Gold-cobalt Nanoparticle Alloys Exhibiting Tunable Compositions, Near-infrared Emission, and High T_2 Relaxivity. *Adv. Funct. Mater.* **2014**, *24* (41), 6532−6539.

(14) Wilson, R. H.; Nadeau, K. P.; Jaworski, F. B.; Tromberg, B. J.; Durkin, A. J. Review of Short-Wave Infrared Spectroscopy and Imaging

Methods for Biological Tissue Characterization. *J. Biomed. Opt.* **2015**, *20* (3), No. 030901.

(15) Chen, Y.; Wang, S.; Zhang, F. Near-Infrared Luminescence High-Contrast in Vivo Biomedical Imaging. *Nat. Rev. Bioeng* **2023**, *1* (1), 60−78.

(16) Cao, F.; Liu, L.; Li, L. Short-Wave Infrared Photodetector. *Mater. Today (Kidlington)* **2023**, *62*, 327−349.

(17) Wu, S.; Han, G.; Milliron, D. J.; Aloni, S.; Altoe, V.; Talapin, D. V.; Cohen, B. E.; Schuck, P. J. Non-Blinking and Photostable Upconverted Luminescence from Single Lanthanide-Doped Nanocrystals. *Proc. Natl. Acad. Sci. U. S. A.* **2009**, *106* (27), 10917−10921.

(18) Nam, S. H.; Bae, Y. M.; Park, Y. I.; Kim, J. H.; Kim, H. M.; Choi, J. S.; Lee, K. T.; Hyeon, T.; Suh, Y. D. Long-Term Real-Time Tracking of Lanthanide Ion Doped Upconverting Nanoparticles in Living Cells. *Angew. Chem., Int. Ed. Engl.* **2011**, *50* (27), 6093−6097.

(19) Pedroso, C. C. S.; Mann, V. R.; Zuberbühler, K.; Bohn, M.-F.; Yu, J.; Altoe, V.; Craik, C. S.; Cohen, B. E. Immunotargeting of Nanocrystals by SpyCatcher Conjugation of Engineered Antibodies. *ACS Nano* **2021**, *15* (11), 18374−18384.

(20) Chan, E. M.; Han, G.; Goldberg, J. D.; Gargas, D. J.; Ostrowski, A. D.; Schuck, P. J.; Cohen, B. E.; Milliron, D. J. Combinatorial Discovery of Lanthanide-Doped Nanocrystals with Spectrally Pure Upconverted Emission. *Nano Lett.* **2012**, *12* (7), 3839−3845.

(21) Gargas, D. J.; Chan, E. M.; Ostrowski, A. D.; Aloni, S.; Altoe, M. V. P.; Barnard, E. S.; Sanii, B.; Urban, J. J.; Milliron, D. J.; Cohen, B. E.; Schuck, P. J. Engineering Bright Sub-10-nm Upconverting Nanocrystals for Single-Molecule Imaging. *Nat. Nanotechnol.* **2014**, *9* (4), 300−305.

(22) Teitelboim, A.; Tian, B.; Garfield, D. J.; Fernandez-Bravo, A.; Gotlin, A. C.; Schuck, P. J.; Cohen, B. E.; Chan, E. M. Energy Transfer Networks within Upconverting Nanoparticles Are Complex Systems with Collective, Robust, and History-Dependent Dynamics. *J. Phys. Chem. C* **2019**, *123* (4), 2678−2689.

(23) Levy, E. S.; Tajon, C. A.; Bischof, T. S.; Iafrati, J.; Fernandez-Bravo, A.; Garfield, D. J.; Chamanzar, M.; Maharbiz, M. M.; Sohal, V. S.; Schuck, P. J.; Cohen, B. E.; Chan, E. M. Energy-Looping Nanoparticles: Harnessing Excited-State Absorption for Deep-Tissue Imaging. *ACS Nano* **2016**, *10* (9), 8423−8433.

(24) Lee, C.; Xu, E. Z.; Liu, Y.; Teitelboim, A.; Yao, K.; Fernandez-Bravo, A.; Kotulska, A. M.; Nam, S. H.; Suh, Y. D.; Bednarkiewicz, A.; Cohen, B. E.; Chan, E. M.; Schuck, P. J. Giant Nonlinear Optical Responses from Photon-Avalanching Nanoparticles. *Nature* **2021**, *589* (7841), 230−235.

(25) Lee, C.; Xu, E. Z.; Kwock, K. W. C.; Teitelboim, A.; Liu, Y.; Park, H. S.; Ursprung, B.; Ziffer, M. E.; Karube, Y.; Fardian-Melamed, N.; Pedroso, C. C. S.; Kim, J.; Pritzl, S. D.; Nam, S. H.; Lohmueller, T.; Owen, J. S.; Ercius, P.; Suh, Y. D.; Cohen, B. E.; Chan, E. M.; Schuck, P. J. Indefinite and Bidirectional Near-Infrared Nanocrystal Photoswitching. *Nature* **2023**, *618* (7967), 951−958.

(26) Takeuchi, T.; Iizumi, Y.; Yudasaka, M.; Kizaka-Kondoh, S.; Okazaki, T. Characterization and Biodistribution Analysis of Oxygen-Doped Single-Walled Carbon Nanotubes Used as in Vivo Fluorescence Imaging Probes. *Bioconjugate Chem.* **2019**, *30* (5), 1323−1330.

(27) Cheng, X.; Pan, Y.; Yuan, Z.; Wang, X.; Su, W.; Yin, L.; Xie, X.; Huang, L. Er^{3+} Sensitized Photon Upconversion Nanocrystals. *Adv. Funct. Mater.* **2018**, *28* (22), No. 1800208.

(28) Liu, L.; Wang, S.; Zhao, B.; Pei, P.; Fan, Y.; Li, X.; Zhang, F. Er3+ Sensitized 1530 Nm to 1180 nm Second Near-Infrared Window Upconversion Nanocrystals for in Vivo Biosensing. *Angew. Chem. Weinheim Bergstr. Ger.* **2018**, *130* (25), 7640−7644.

(29) Skripka, A.; Lee, M.; Qi, X.; Pan, J.-A.; Yang, H.; Lee, C.; Schuck, P. J.; Cohen, B. E.; Jaque, D.; Chan, E. M. A Generalized Approach to Photon Avalanche Upconversion in Luminescent Nanocrystals. *Nano Lett.* **2023**, *23* (15), 7100−7106.

(30) Shalav, A.; Richards, B. S.; Trupke, T.; Krämer, K. W.; Güdel, H. U. Application of NaYF4:Er3+ up-Converting Phosphors for Enhanced near-Infrared Silicon Solar Cell Response. *Appl. Phys. Lett.* **2005**, *86* (1), No. 013505.

(31) Antaris, A. L.; Chen, H.; Cheng, K.; Sun, Y.; Hong, G.; Qu, C.; Diao, S.; Deng, Z.; Hu, X.; Zhang, B.; Zhang, X.; Yaghi, O. K.; Alamparambil, Z. R.; Hong, X.; Cheng, Z.; Dai, H. A Small-Molecule Dye for NIR-II Imaging. *Nat. Mater.* **2016**, *15* (2), 235−242.

(32) Wang, S.; Fan, Y.; Li, D.; Sun, C.; Lei, Z.; Lu, L.; Wang, T.; Zhang, F. Anti-Quenching NIR-II Molecular Fluorophores for in Vivo High-Contrast Imaging and pH Sensing. *Nat. Commun.* **2019**, *10* (1), 1058.

(33) Yang, B.; Yu, Y.; Zhang, G.; Shao, X.; Li, X. Design and Fabrication of Broadband InGaAs Detectors Integrated with Nanostructures. *Sensors* **2023**, *23* (14), 6556.

(34) Chen, D.; Lei, L.; Yang, A.; Wang, Z.; Wang, Y. Ultra-Broadband Near-Infrared Excitable Upconversion Core/Shell Nanocrystals. *Chem. Commun.* **2012**, *48* (47), 5898−5900.

(35) Zhou, B.; Tang, B.; Zhang, C.; Qin, C.; Gu, Z.; Ma, Y.; Zhai, T.; Yao, J. Enhancing Multiphoton Upconversion through Interfacial Energy Transfer in Multilayered Nanoparticles. *Nat. Commun.* **2020**, *11* (1), 1174.

(36) Liu, S.; Yan, L.; Huang, J.; Zhang, Q.; Zhou, B. Controlling Upconversion in Emerging Multilayer Core−Shell Nanostructures: From Fundamentals to Frontier Applications. *Chem. Soc. Rev.* **2022**, *51* (5), 1729−1765.

(37) Chan, E. M.; Levy, E. S.; Cohen, B. E. Rationally Designed Energy Transfer in Upconverting Nanoparticles. *Adv. Mater.* **2015**, *27* (38), 5753−5761.

(38) Ribet, S. M.; Varnavides, G.; Pedroso, C.; Cohen, B. E. Uncovering the Three-Dimensional Structure of Upconverting Core−Shell Nanoparticles with Multislice Electron Ptychography. *Appl. Phys. Lett.* **2024**, *124*, No. 240601.

(39) Pollnau, M.; Gamelin, D. R.; Lüthi, S. R.; Güdel, H. U.; Hehlen, M. P. Power Dependence of Upconversion Luminescence in Lanthanide and Transition-Metal-Ion Systems. *Phys. Rev. B Condens. Matter* **2000**, *61* (5), 3337−3346.

(40) Würth, C.; Fischer, S.; Grauel, B.; Alivisatos, A. P.; Resch-Genger, U. Quantum Yields, Surface Quenching, and Passivation Efficiency for Ultrasmall Core/Shell Upconverting Nanoparticles. *J. Am. Chem. Soc.* **2018**, *140* (14), 4922−4928.

(41) Liu, H.; Xu, C. T.; Lindgren, D.; Xie, H.; Thomas, D.; Gundlach, C.; Andersson-Engels, S. Balancing Power Density Based Quantum Yield Characterization of Upconverting Nanoparticles for Arbitrary Excitation Intensities. *Nanoscale* **2013**, *5* (11), 4770−4775.

(42) Labrador-Páez, L.; Kostiv, U.; Liu, Q.; Li, Y.; Ågren, H.; Widengren, J.; Liu, H. Excitation Pulse Duration Response of Upconversion Nanoparticles and Its Applications. *J. Phys. Chem. Lett.* **2022**, *13* (48), 11208−11215.

(43) Fardian-Melamed, N.; Skripka, A.; Lee, C.; Ursprung, B.; Darlington, T. P.; Teitelboim, A.; Qi, X.; Wang, M.; Gerton, J. M.; Cohen, B. E.; Chan, E. M.; Schuck, P. J. Infrared Nanosensors of Pico-to Micro-Newton Forces. *arXiv [physics.optics]*, **2024**. http://arxiv.org/abs/2404.02026.

(44) Skripka, A.; Zhang, Z.; Qi, X.; Ursprung, B.; Ercius, P.; Cohen, B. E.; Schuck, P. J.; Jaque, D.; Chan, E. M. Intrinsic Optical Bistability of Photon Avalanching Nanocrystals. *arXiv [physics.optics]*, **2024**. http://arxiv.org/abs/2403.04098.